Crystal-Arrested Phase Separation

Juan Sabin, Arthur E. Bailey, Gabriel Espinosa, and Barbara J. Frisken

Phys. Rev. Lett. **109**, 195701 — Published 7 November 2012

DOI: 10.1103/PhysRevLett.109.195701

Crystal-arrested phase separation

Juan Sabin,[1,*] Arthur E. Bailey, Gabriel Espinosa,[1,†] and Barbara J. Frisken[1]

[1] *Department of Physics, Simon Fraser University, Burnaby BC V5A 1S6*

(Dated: September 19, 2012)

Abstract

We have studied the interplay between phase separation and crystallization in a colloid-polymer mixture along one kinetic pathway in samples which exhibit three-phase equilibrium coexistence. In analogy with atomic systems, the range of the effective attractive interaction between colloids is sufficiently long to allow for a stable liquid phase. By direct imaging in microgravity on the International Space Station, we observe a unique structure, a 'crystal gel', that occurs when gas-liquid phase separation arrests due to crystallites within the liquid domain spanning the cell. From the initial onset of spinodal decomposition until arrest caused by this structure, the kinetics of phase separation remain largely unaffected by the formation of the third phase. This dynamic arrest appears to result from the stiffness of the crystalline strands exceeding the liquid-gas interfacial tension.

PACS numbers: 64.70.dg, 64.75.Xc

Mixtures of colloids and non-adsorbing polymers have been investigated extensively as a convenient model for a wide variety of fundamental properties of matter including phase behavior and phase transition kinetics [1, 2]. The great flexibility of this system results from the tunable nature of the effective attractive interaction induced by the entropy of polymer added to a hard-sphere colloidal suspension. The dimensionless range of this interaction ξ is defined as the ratio of the polymer's size to the colloidal particle size, and the strength of the interaction is set by the polymer concentration [3, 4]. At a sufficiently long range of attraction, $\xi > 0.3$, the colloid-polymer (C-P) system exhibits a phase diagram including a region of triple coexistence of colloid-poor (gas), colloid-rich (liquid) and colloidal solid (crystal) phases [5]. In addition, the kinetics of phase separation in the region of coexistence of gas and liquid phases of the C-P samples are nearly identical to those of simple liquids or liquid mixtures with the colloid size determining the governing length scale [6]. These factors make the colloid-polymer mixture system a nearly ideal one in which to explore the kinetics of phase separation in the presence of three-phase coexistence.

Multiple routes to complete phase separation exist within the three-phase region but sedimentation limits observation of fundamental phenomena. Investigations of three-phase C-P phase separation have revealed a variety of kinetic pathways [7]. These kinetic regimes can be described in terms of the free-energy landscape of the system [8]. One pathway, in particular, referred to as regime G [7], begins with gas-liquid phase separation followed by nucleation of crystals within the liquid phase. This occurs in the low- to mid-colloid volume fraction region of the three-phase triangle, centered between the underlying gas-liquid binodals. On Earth, gravity causes sedimentation of the crystals and stratification of the three phases. While gravity may not affect the early stages of this process, the later stages must surely evolve differently without gravity. In this Letter, we report the detailed kinetics of this regime studied both on Earth and in microgravity on the International Space Station (ISS).

We prepared samples exhibiting three-phase coexistence at constant interaction range. Polymethylmethacrylate (PMMA) spheres, sterically stabilized by a thin surface layer of poly-12-hydroxystearic acid [9], were suspended in a 45:55 by mass mixture of decahydronaphthalene (decalin) and tetrahydronaphthalene (tetralin). This mixture nearly matches the refractive index of the colloidal particles and reduces van der Waals attraction. The PMMA particles were heat-shocked to ensure equilibrium swelling caused by tetralin ad-

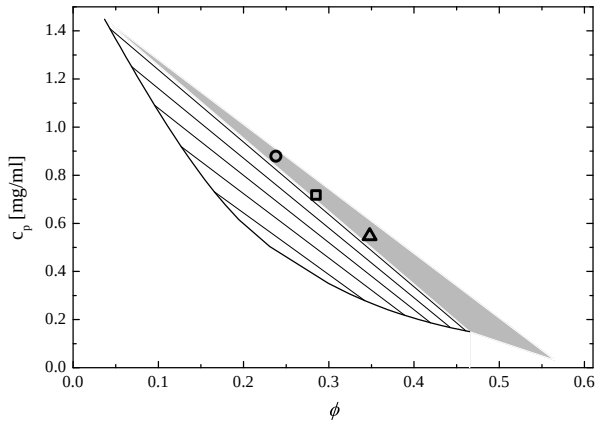

FIG. 1. Schematic phase diagram of the C-P system graphed as polymer concentration c_p vs colloid volume fraction ϕ. The diagram is calculated from a mean-field analytic approximation [12]. The shaded triangle shows the three-phase coexistence region; the curve is the two-phase gas-liquid coexistence curve with several tie-lines shown. Samples 1 (◯), 2 (□) and 3 (△), have $\phi = 0.24$, 0.29, and 0.35 and $c_p = 0.88$, 0.72, and 0.55 mg/mL, respectively.

sorption [10]. The colloidal particles were measured by static light scattering to have a 229 nm radius. Polystyrene (PS), molecular weight M_w = 13.2 x 10^6 g·mol^{-1} and heterogeneity $M_w/M_n = 1.05$ (Polymer Laboratories Ltd., UK), was added to the solvent mixture, which is somewhat better than a theta solvent for PS [1, 11]. Static light scattering from the polymer in the solvent mixture measured a radius of gyration of 120 nm, yielding $\xi = 0.52$. The cocentrations of the samples are shown in the phase diagram of Fig. 1.

On Earth, these samples show the kinetics described by Renth and coworkers for samples within regime G [7]. After homogenization, taken as time $t = 0$, a rapid increase of the turbidity occurs, followed by formation of a diffuse interface between colloid-poor and colloid-rich phases. This interface sharpens and moves towards the bottom of the cell over time. The first crystals appear in the liquid phase within 6 hours and slowly settle forming a crystal phase in the bottom of the cell. No significant evolution of the samples occurs after 40 hours.

The colloid-polymer samples were studied in microgravity using the Binary Colloidal Alloy Test 5 (BCAT-5) instrumentation. The samples were sealed into glass cuvettes (Hellma) having a visible volume 4 x 10 x 20 mm, and placed in a holder with optical-quality windows and launched via Space Shuttle to the ISS. Working one sample at a time, each sample was

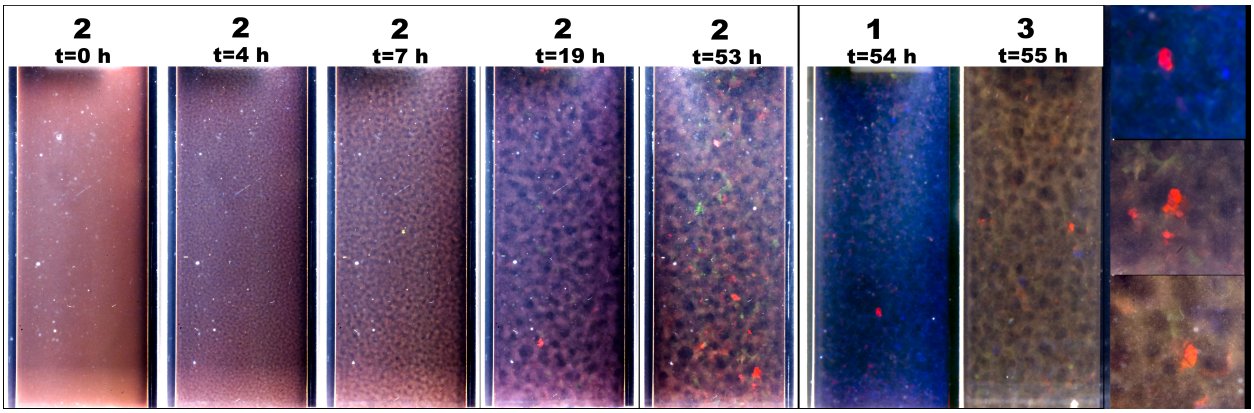

FIG. 2. (Color online) Images of the samples in microgravity. The left five images show Sample 2 evolving from time t=0 to t=53 h. Domains in the 19 h and 53 h images have exactly the same pattern. Crystal visibility was improved in the 53 h image by an illumination change. The two images to the right show the other two samples at comparable times. Each of these seven images shows the full width of the cuvette. The three images on the far right show a 2.5 mm wide region of each sample with a prominate crystal: Sample 1 at the top to Sample 3 at the bottom. The crystal size is comparable to the liquid domain size.

homogenized by repeatedly dragging a magnetic stirbar through it for about 20 min. Subsequently, the sample was imaged using a Kodak DCS760 camera with a Nikon AF-S Micro Nikkor 105 mm F2.8G macro lens and a Nikon SB-800 flash at regular intervals for several days. The flash provided transmission illumination of the sample at an angle $\sim 60^\circ$ relative to the camera lens. Each sequence of photographs was cropped, converted to grey scale and contrast enhanced using Adobe After Effects CS4 software. [13]

The images show coarsening of phase separated domains until an arrest stops further evolution. Figure 2 shows a sequence of images taken of Sample 2. The $t = 0$ image shows the sample just after mixing. A bicontinuous network of light and dark regions characteristic of spinodal decomposition becomes evident by 4 h. As the phases evolve, the domain size increases until approximately 20 h after mixing, when domain growth halts. Crystals are first visible approximately 7 h after mixing, similar to Earth-bound experiments, and subsequently additional crystals grow in the liquid phase throughout the sample. Crystal growth continues until the maximum crystallite size is comparable to the liquid domain size. [14] As seen in the time-lapse video of the sample, [14] the crystals move and rotate prior to sample arrest but remain motionless after. The right end of the figure shows the

arrested structure of each sample. This structure is quite stable; photographs of Sample 2 taken one year after homogenization show the same characteristic domain size.

The characteristic length-scale L of the phase separation process, representing the domain spacing, was determined by locating the nearest-neighbor peak in the azimuthally averaged 2-D correlation function calculated from each image using a method previously described. [6] Evolution of L is shown for all three samples in Fig. 3. All three samples show initial power law growth of L with an exponent close to 1, characteristic of phase separation driven by minimization of the interfacial area. The final domain spacing for Samples 2 and 3 is 1.2 mm, less than 1/3 of the shortest dimension of the cuvette. Sample 1 shows a final domain spacing about 30% smaller than that of the other two samples.

The microgravity results agree with and extend Earth-bound measurements. Small-angle light scattering (SALS) was measured on Earth using a custom setup with an angular range from 0.08 to 10 degrees. [15] Immediately after homogenization, a scattering ring appears with a maximum at a scattering wavevector $q_m = \frac{4\pi n}{\lambda} \sin(\theta_m/2)$, where n is the refractive index, λ is the laser's wavelength, and θ_m is the scattering angle at which the maximum intensity occurs. This dominant wavevector is related to a characteristic length scale of colloid concentration fluctuations by $L \approx 2\pi/q_m$. After fitting a Gaussian function to a limited number of points near the scattered peak to determine q_m, the resulting L data are graphed in Fig. 3. These results, combined with microgravity results, are shown in the left graph of Fig. 3 with time scaled by the characteristic time τ and L by the colloid diameter d. The characteristic time is given by $\tau = k_B T/(6\pi\eta d^3)$ where the viscosity η was estimated as that of the polymer-solvent mixture in the free volume of each sample. [6] Scattering during the initial stages of phase separation shows L grows as $t^{1/3}$, characteristic of diffusion-limited spinodal decomposition. At intermediate times, the growth rate increases, consistent with phase separation driven by minimization of the interfacial area. [16] At $t/\tau \sim 100$, gravity accelerates growth as sedimentation severely increases the speed of coalescence. The microgravity image data, however, demonstrate that without sedimentation L continues to coarsen with a growth law close to t^1. The combination of SALS and microgravity data agrees well with the empirical expression proposed by Furukawa [17] for phase separation of binary fluids (dashed line) until the phase separation arrests. The same values of the adjustable parameters in this expression $A = 0.14$ and $B = 0.022$ were used as resulted from experiments in binary liquids [17], simple liquids [18], and the two phase region of a C-P

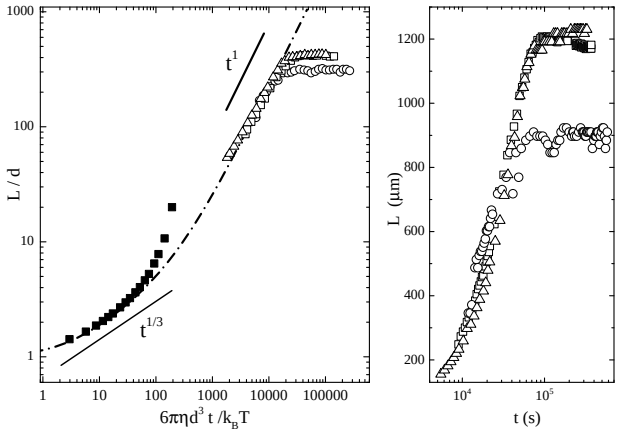

FIG. 3. Time dependence of characteristic length scale for all samples. The right-hand, semi-log graph shows results from the microgravity samples 1 (◯), 2 (□) and 3 (△). The left-hand log-log graph shows the reduced time vs reduced length scale for the microgravity samples and scattering measurements (■) from a sample similar to sample 2 in 1-g. The Furukawa function is shown with a dash-dot line.

sample [6], and similar to the values found for polymer blends [19]. The kinetics from the onset of spinodal decomposition until nearly the time of arrest remain largely unaffected by the formation of the third phase.

The novel final-state structure observed in microgravity can be interpreted as a "cyrstal gel" where phase separation arrests due to crystal growth resulting in a network of crystals spanning the sample volume. This final state is not the expected equilibrium state resulting from complete phase separation in which we expect the three phases to be fully separated and interfacial area minimized, likely with either the liquid or crystal phases wetting the sample cell [6]. We suggest that kinetic arrest results from the crystalline deformation energy exceeding the surface tension energy so significantly that the probability of further coarsening becomes exceedingly low. If sufficient crystallinity develops within the tube-like liquid domain, crystal impingement and fusion will occur and the yield modulus of the solid phase comes into play. Prior to this, the gas-liquid interfacial tension could move the crystallites, as observed in the time-lapse video, with viscous losses but without an energy barrier.

The crystalline elastic energy can be compared to the gas-liquid interfacial energy by considering a crystalline cylinder with radius r surrounded by a layer of colloidal liquid of

thickness Δ. The total elastic energy for a tube of crystallites with length l at maximum elastic strain is $U_e = \pi r^2 l \delta_L^2 G_o/2$, where we take the maximum elastic strain as the Lindemann parameter δ_L [20] and G_o is the elastic modulus of the crystal. Following an argument used for hard sphere colloids [20], we assume the elastic energy per particle results from a dominant energy scale in the system $\epsilon_g k_B T$, yielding the product $\delta_L^2 G_o = (3\phi_c/16\pi a^3)\epsilon_g k_B T$. Comparing the elastic energy with the total surface energy, $2\pi l(r+\Delta)\epsilon_i \phi_l k_B T/a^2$ [21] where ϕ_l is the liquid-phase colloid volume fraction and ϵ_i is the energy scale for interfacial tension, we find that the surface energy exceeds the elastic deformation energy when

$$\frac{\Delta}{r} > \frac{3}{64\pi}\left(\frac{\phi_c}{\phi_l}\right)\left(\frac{r}{a}\right)\left(\frac{\epsilon_g}{\epsilon_i}\right) - 1. \tag{1}$$

Since the colloid-polymer system has a single dominant energy, the interaction energy, $\epsilon_g = \epsilon_i$.The values $\phi_l = 0.47$ and $\phi_c = 0.57$ result from the theoretical phase diagram. From our images, we find typical crystal sizes $2r \sim 350\mu$m; thus, the liquid layer would need to be at least 2200μm thick to have sufficient surface energy to exceed the elastic energy. This large value results from the layer thickness scaling as the square of the crystal size and from the large crystal size, $r/a \sim 750$, at the time of arrest.

This arrest mechanism likely applies only for samples for which the kinetic path begins via spinodal decomposition, generating a bicontinuous domain network, and sufficient crystallinity is present. Without the bicontinuous structure, crystalline strands cannot form a semi-rigid structure spanning the sample. In the case of nucleated liquid droplets containing crystals, for example, the droplets would be free to coalesce, continually reducing surface energy without arrest. Even if a bicontinuous gas-liquid domain network forms, arrest will occur only if the crystalline strands form, thus, requiring a minimum crystallinity within the liquid-crystal domains. In fact, equation (1) for the relative thickness of the liquid layer has a critical value. For sufficiently small crystalline strands, an infinitesimal amount of liquid coating would be sufficient to overcome the yield modulus. From our approximation, the critical crystalline strand radius for our samples in units of the colloid size r/a is ~ 55. Therefore, within the limitations of this simple model, crystalline strands smaller than approximately 110 colloids across cannot form a "crystal gel".

The smaller characteristic size at arrest in Sample 1 results from earlier arrest of this sample compared to the others. This may result from the significantly smaller liquid phase volume in this sample as was observed on Earth and evidenced by Sample 1's close proximity

to the gas-solid boundary of the three-phase region. As domain coarsening proceeds, the initially liquid domain is simultaneously being partially consumed by crystallization. The arrest time is likely set by the shrinking liquid phase volume sufficiently confining the crystals causing crystalline strand formation, which occurs earlier in samples with a lower liquid to crystal phase volume ratio.

The arrest observed in this regime of the three-phase region is reminiscent of gelation of C-P mixtures at higher interaction strengths. Systems with a short range of attraction ($\xi < 0.2$) and intermediate interaction strengths and colloid concentrations gel via phase separation due to a metastable gas-liquid coexistence within the region of gas-crystal coexistence in the phase diagram [1]. Arrest occurs when the dense phase reaches a gelation boundary [22]. Systems with a longer range of attraction exhibit similar behavior, forming both stable [23] and unstable [24] gels. Gelation is expected at higher interaction potential because the strength of the interaction prevents rearrangement of the particles after contact, resulting in an amorphous non-equilibruium structure. In contrast, the arrest reported here occurs in a region where equilibrium is a three-phase state.

Experimentation in microgravity has revealed the fundamental behaviour of this system. The kinetic pathway is confirmed but the small surface forces, which are overwhelmed in Earth's gravity, play a major role and lead to the formation of a unique crystal gel structure. The phases observed reach their final concentrations, but macroscopic phase separation is not achieved because the interfacial energy between the two lower-density phases is insufficient to overcome the stiffness of the crystalline strands. This effect may occur in any three-phase system whose interfacial and elastic energies result from a single dominant system energy scale. Further investigation of other kinetic pathways may yield further insights into the details of phase separation in the presence of three phases.

We gratefully acknowledge contributions by astronauts Robert Thirsk and Shannon Walker, the Canadian Space Agency (CSA) and NASA BCAT-5 teams, particularly Charles Gauthier; David Lee (SALS experiments), Peter Lu (sample preparation and data analysis guidance), and Andrew Hollingworth (colloid synthesis). We thank David Weitz, Wilson Poon and Veronique Trappe for helpful discussions. Financial support was received from the CSA, the Spanish Government, and NSERC of Canada.

* Current Address: Biophysics and Interfaces Group, Department of Applied Physics, University of Santiago de Compostela, E-15782 Santiago de Compostela, Spain

† Current Address: Instituto de Física y Matemáticas, Universidad Michoacana de San Nicolás de Hidalgo, Edificio C3-B, Ciudad Universitaria, C.P. 58060, Morelia, Michoacán, Mexico

[1] W. C. K. Poon, J. Phys: Condens. Matter **14**, R859 (2002).

[2] V. J. Anderson and H. N. W. Lekkerkerker, Nature **416**, 811 (2002).

[3] A. Vrij, Pure & Appl. Chem. **48**, 471 (1976).

[4] F. Oosawa and S. Asakura, J. Chem. Phys. **22**, 1255 (1954).

[5] H. N. W. Lekkerkerker, W. C. K. Poon, A. Stroobants, and P. B. Warren, Europhys. Lett. **20**, 559 (1992).

[6] A. E. Bailey, W. C. K. Poon, R. J. Christianson, A. B. Schofield, U. Gasser, V. Prasad, S. Manley, P. N. Segre, L. Cipelletti, W. V. Meyer, M. P. Doherty, S. Sankaran, A. L. Jankovsky, W. L. Shiley, J. P. Bowen, J. C. Eggers, C. Kurta, T. Lorik, Jr, P. N. Pusey, and D. A. Weitz, Phys. Rev. Lett. **99**, 205701 (2007).

[7] F. Renth, W. C. K. Poon, and R. M. L. Evans, Phys. Rev. E **64**, 031402 (2001).

[8] R. M. L. Evans, W. C. K. Poon, and F. Renth, Phys. Rev. E **64**, 031403 (2001).

[9] M. T. Elsesser and A. D. Hollingsworth, Langmuir **26**, 17898 (2010).

[10] S.-E. Phan, W. B. Russel, Z. Cheng, J. Zhu, P. M. Chaikin, J. H. Dunsmuir, and R. H. Ottewill, Phys. Rev. E **54**, 6633 (1996).

[11] ed. J. E. Mark, *Physical Properties of Polymers Handbook, 2nd Edition* (Springer Science + Business Media, New York, 2007).

[12] G. J. Fleer and R. Tuinier, Adv. Coll. Int. Sci. **143**, 1 (2008).

[13] P. J. Lu, *Gelation and Phase Separation of Attractive Colloids*, Ph.D. thesis, Harvard University (2008).

[14] See EPAPS Document No. [*Publiser to insert*] for a time-lapse video of the evolution of Sample 2. Note motion of crystals prior to arrest. For more information on EPAPS, see http://www.aip.org/pubservs/epaps.html.

[15] D. Lee, I. A. Gutowski, A. E. Bailey, L. Rubatat, J. R. de Bruyn, and B. J. Frisken, Phys. Rev. E **83**, 031401 (2011).

[16] V. S. Nikolayev, D. Beysens, and P. Guenoun, Phys. Rev. Lett. **76**, 3144 (1996).

[17] P. Guenoun, R. Gastaud, F. Perrot, and D. Beysens, Phys. Rev. A **36**, 4876 (1987).

[18] Y. Garrabos, B. L. Neindre, P. Guenoun, B. Khalil, and D. Beysens, Europhys. Lett. **19**, 491 (1992).

[19] F. S. Bates and P. Wiltzius, J. Chem. Phys. **91**, 3258 (1989).

[20] Z. Cheng, J. Zhu, W. B. Russel, and P. M. Chaikin, Phys. Rev. Lett. **85**, 1460 (2000).

[21] E. H. A. de Hoog and H. N. W. Lekkerkerker, J. Phys. Chem. B **103**, 5274 (1999).

[22] W. C. K. Poon and M. D. Haw, Adv. Coll. Int. Sci. **73**, 71 (1997); P. J. Lu, E. Zaccarelli, F. Ciulla, A. B. Schofield, F. Sciortino, and D. A. Weitz, Nature **453**, 499 (2008); E. Zaccarelli, P. J. Lu, F. Ciulla, D. A. Weitz, and F. Sciortino, J. Phys.: Condens. Matter **20**, 494242 (2008); T. Gibaud and P. Schurtenberger, *ibid.* **21**, 322201 (2009); F. Cardinaux, T. Gibaud, A. Stradner, and P. Schurtenberger, Phys. Rev. Lett. **99**, 118301 (2007).

[23] J. C. Conrad, H. M. Wyss, V. Trappe, S. Manley, K. Miyazaki, L. J. Kaufman, A. B. Schofield, D. R. Reichman, and D. A. Weitz, J. Rheol. **54**, 421 (2010).

[24] L. J. Teece, M. A. Faers, and P. Bartlett, Soft Matter **7**, 1341 (2011).